http://dx.doi.org/10.5012/bkcs.2014.35.5.1516

The Coating Effects of Al_2O_3 on a $Li[Li_{0.2}Mn_{0.54}Co_{0.13}Ni_{0.13}]O_2$ Surface Modified with $(NH_4)_2SO_4$

Ji-Woo Oh, Rye-Gyeong Oh, Jung-Eui Hong, Won-Geun Yang, and Kwang-Sun Ryu*

*Department of Chemistry, University of Ulsan, Ulsan 680-749, Korea. *E-mail: ryuks@ulsan.ac.kr*
Received September 27, 2013, Accepted January 30, 2014

A series of 20 wt % $(NH_4)_2SO_4$ and 3 wt % Al_2O_3 surface treatments were applied to $Li[Li_{0.2}Mn_{0.54}Co_{0.13}Ni_{0.13}]O_2$ substrates. The $Li[Li_{0.2}Mn_{0.54}Co_{0.13}Ni_{0.13}]O_2$ substrates were synthesized using a co-precipitation method. Sample (a) was left pristine and variations of the 20 wt % $(NH_4)_2SO_4$ and 3 wt % Al_2O_3 were applied to samples (b), (c) and (d). XRD was used to verify the space group of the samples as $R\bar{3}m$. Additional morphology and particle size data were obtained using SEM imagery. The Al_2O_3 coating layers of sample (b) and (d) were confirmed by TEM images and EDS mapping of the SEM images. 2032-type coin cells were fabricated in a glove box in order to investigate their electrochemical properties. The cells were charged and discharged at room temperature (25 ºC) between 2.0V and 4.8V during the first cycle. The cells were then charged and discharged between 2.0V and 4.6V in subsequent cycles. Sample (d) exhibited lower irreversible capacity loss (ICL) in the first charge-discharge cycle as compared to sample (c). Sample (d) also had a higher discharge capacity of ~250 mAh/g during the first and second charge-discharge cycles when compared with sample (c). The rate capability of the Al_2O_3-coated sample (b) and (d) was lower when compared with sample (a) and (c). Sample (d), coated with Al_2O_3 after the surface treatment with $(NH_4)_2SO_4$, showed an improvement in cycle performance as well as an enhancement of discharge capacity. The thermal stability of sample (d) was higher than that of the sample (c) as the result of DSC.

Key Words : Lithium-ion battery, Cathode, Over lithiation oxide, Surface treatments

Introduction

The layered $LiCoO_2$ has received extensive interest, however, it suffers from the low energy density, high cost, and toxicity. In this regard, solid solutions between layered $Li(Li_{1/3}Mn_{2/3})O_2$ (commonly designated as Li_2MnO_3) and $LiMO_2$ (M = Mn, Co, Ni) have become an area of increased interest in recent years, as they offer high capacities about 250 mAh/g with a significant reduction in cost and improvement in safety when compared to the $LiCoO_2$ cathode.[1-5] These materials have the potential to increase the overall capacity and energy density of Li ion batteries; however, the high discharge capacity of the materials is only available at a low discharge rate (typically C/20). When the discharge current is increased, the available discharge capacity of the materials is drastically reduced, with a typical discharge capacity below 200 mAh/g at a 1C rate.[6-8] This is due to the creation of sites of two-dimensional (2D) diffusion-layered structures, and because the rate capability of a material is generally affected by bulk Li diffusion and transport through the surface of the particles. Recently, it has been determined that rate ability can be enhanced with $(NH_4)_2SO_2$ treatment. Li-excess Mn-based layered materials treated with $(NH_4)_2SO_2$ have a surface structure similar to the spinel. Spinel structure, as in $LiMn_2O_4$, $LiNi_{0.5}Mn_{1.5}O_4$, and $Li_4Mn_5O_{12}$, has a three-dimensional (3D) diffusion path and good reversibility of Li-ion intercalation or deintercalation. Spinel structure is also structurally compatible with layered structure, with the same oxygen arrangement, and differs only in the arrangement of Li and transition-metal atoms. The two structures can thus be integrated without a distinct boundary.[9-11] According to previous study, the active material treated with 20 wt % $(NH_4)_2SO_2$ exhibited a better enhanced discharge capacity and rate ability than among various percentage of $(NH_4)_2SO_2$ as amounts. The improvement in cycle performance, however, was not significant, indicating that surface treatment does not significantly affect cycle performance, since the surface treatment method does not insulate the active material from direct contact with the electrolyte. It is clear that the structure of the surface is of great importance to the electrochemical performance of cathode materials. Therefore, additional surface coating is required to improve cycle performance. As a coating material, Al_2O_3 can prevent the direct contact of electrolyte with cathode materials and it shows the best cyclability on the spinel structure among MgO, TiO_2, ZrO_2, and other compounds or composites, according to the preceded researches.[12] In addition, surface modification of active materials by Al_2O_3 is needed to achieve higher thermal stability.[13] But Al_2O_3 has no conductivity and no ability for capacity. Minimum amount of Al_2O_3 for best performance was revealed below 3% as molar ratios from previous study.

In this study, in order to improve the cycle-life and thermal stability of $Li[Li_{0.2}Mn_{0.54}Co_{0.13}Ni_{0.13}]O_2$ substrates treated with $(NH_4)_2SO_4$, the substrates were surface-coated with Al_2O_3. To measure the coating effect of Al_2O_3 on the $Li[Li_{0.2}Mn_{0.54}Co_{0.13}Ni_{0.13}]O_2$ surface modified by $(NH_4)_2SO_4$, we compared the electrochemical performance of four

samples: $Li[Li_{0.2}Mn_{0.54}Ni_{0.13}Co_{0.13}]O_2$ pristine (sample (a)), Al_2O_3-modified $Li[Li_{0.2}Mn_{0.54}Ni_{0.13}Co_{0.13}]O_2$ (sample (b)), $(NH_4)_2SO_4$-treated $Li[Li_{0.2}Mn_{0.54}Ni_{0.13}Co_{0.13}]O_2$ (sample (c)), and Al_2O_3-modified $Li[Li_{0.2}Mn_{0.54}Ni_{0.13}Co_{0.13}]O_2$ treated with $(NH_4)_2SO_4$ (sample (d)). We expect enhanced cyclability and thermal stability in sample (d), due to bulwarks against electrolytes from the Al_2O_3 surface coating.

Experimental

Lithium hydroxide monohydrate (assay ≥ 98.0%), manganese (II) acetate tetrahydrate (assay ≥ 99.0%), nickel (II) nitrate hexahydrate (assay ≥ 98.5%), and cobalt (II) acetate tetrahydrate (assay ≥ 98.0%) were purchased from Sigma Chemical Co. All chemicals and solvents used were analytical grade and used as received. Double distilled water was used throughout this study. Sample (a) (pristine) consisted of $Li[Li_{0.2}Mn_{0.54}Co_{0.13}Ni_{0.13}]O_2$ synthesized *via* a co-precipitation method. Required amounts of the transition metal acetates were dissolved in deionized water and added by dropper to a 0.1 M NaOH solution to form the co-precipitated hydroxides of Mn, Co, and Ni. After drying overnight at 100 °C in an air oven, the coprecipitated hydroxides were mixed with a required amount of lithium hydroxide, and fired in air at 900 °C for 24 h. Sample (b) consisted of Al_2O_3-coated $Li[Li_{0.2}Mn_{0.54}Co_{0.13}Ni_{0.13}]O_2$ and was prepared *via* the traditional Al_2O_3 coating process. The $Li[Li_{0.2}Mn_{0.54}Co_{0.13}Ni_{0.13}]O_2$ powder (pristine) was poured into a 3% $Al(NO_3)_3$ solution with continuous stirring for 1 h. The Al content was set at molar ratios of Al/(Ni + Co +Mn) = 3% by controlling the amount of $Al(NO_3)_3$. NH_4OH was then slowly added, and pH was controlled at 8. This mixture was kept at 80 °C for 5 h until most of the solvent was evaporated. The powder was dried at 120 °C for 12 h and sintered at 500 °C for 5 h. Sample (c) consisted of the $Li[Li_{0.2}Mn_{0.54}Co_{0.13}Ni_{0.13}]O_2$ powder (pristine) treated with $(NH_4)_2SO_4$ in water. The amount of $(NH_4)_2SO_4$ used relative to the weight of the active material was $(NH_4)_2SO_4$/$Li[Li_{0.2}Mn_{0.54}Co_{0.13}Ni_{0.13}]O_2$ = 20 wt %. $(NH_4)_2SO_4$ was first dissolved in distilled water. The active material (pristine) was then mixed into the solution and dried at 80 °C. The resulting powder was annealed at 300 °C for 10 h to decompose the $(NH_4)_2SO_4$. The final material was washed with distilled water, filtered, and dried to remove impurities.[2] The $(NH_4)_2SO_4$ surface modification of the thus-treated active material was carried out by dispersing the powders from sample (c) into the 3 wt % $Al(NO_3)_3$ solution, followed by the addition of NH_4OH to precipitate aluminum hydroxide. This process formed sample (d). The products were heated at 500 °C in air for 5 h.

Sample structures were characterized using X-ray powder diffraction (XRD). XRD was performed using the Rigaku ultra-x (Rigaku Co., CuK_α radiation (λ = 1.5418 Å), 40 kV, 120 mA) in the 2θ value range of 15-80° with a step of 0.02° sec^{-1}. Morphology and particle size data were obtained from field emission scanning electron microscopy (FE-SEM, Supra 40, Carl Zeiss Co., Ltd.). The Al_2O_3 coating layers of samples (b) and (d) were confirmed with transmission electron microscopy images (FE-TEM, JEM 2100F, JEOL Ltd., 200 kV) and energy dispersive spectrometer mapping (EDS, Supra 40, Carl Zeiss Co., Ltd.) of the SEM imagery. To measure a reduced amount of lithium by the reaction with $(NH_4)_2SO_4$ in the active materials, the molar ratios of the metal elements present in samples (a) and (c) were evaluated by inductively-coupled plasma emission spectroscopy (ICP, Varian).

The electrodes were prepared by casting and pressing a mixture of 80 wt % of the obtained active material, 10 wt % of PVdF (polyvinylidene difluoride) binder, and 10 wt % of carbon black (Super P) in *N*-methyl pyrrolidinone (NMP) solvent on aluminum foil, followed by drying for 24 h at 80 °C. The coin-type cells (CR 2032) were fabricated in an argon-filled glove box with a 1.15 M $LiPF_6$ electrolyte in an ethylene carbonate-diethyl carbonate-dimethyl carbonate (EC-DEC-DMC, 3:2:5 volume ratio) solution. A celgard 2400 film separated the positive electrode from the lithium metal negative electrode.

To investigate the electrochemical properties, the cells were charged and discharged in the first cycle at room temperature (25 °C) between 2.0 V and 4.8 V. Cells were then charged and discharged between 2.0V and 4.6 V. At this time, the current density of 20 mA/g (0.08 C) was applied. Discharge current densities measured during the rate capability test were 100 mA/g (0.4 C), 200 mA/g (0.8 C), and 300 mA/g (1.2 C). The discharge current of the cycle life test was 300 mA/g (1.2 C), but the charge current density was fixed at 20 mA/g (0.08 C) for both rate capability and cycle life. Cyclic voltammogram (CV, Wonatech) data of the cells were obtained in the range of 2.0-4.8 V at a scan rate of 0.03 mV/s.

The thermal stability of the sample (c) and (d) was measured by using differential scanning calorimetry (DSC, Q20, TA Instruments Co.). For DSC measurements, the Li ion cells were fully charged to 4.8 V, the positive electrode was taken out of the cell, and the electrolyte was wiped with filter paper. A piece of crushed pellet was mechanically sealed in an aluminum cell used to collect samples of approximately 7 mg.

Results and Discussion

Lattice constants of the samples were determined by fitting the peak positions with an $R\bar{3}m$ space group; the results are shown in Table 1. Figure 1(a) shows the fitted XRD peaks of sample (a) (pristine) by rietveld refinement, representatively. Figure 1(b) shows the XRD patterns of $Li[Li_{0.2}Mn_{0.54}Ni_{0.13}Co_{0.13}]O_2$ (sample (a)), Al_2O_3-modified $Li[Li_{0.2}Mn_{0.54}Ni_{0.13}Co_{0.13}]O_2$ (sample (b)), $(NH_4)_2SO_4$-treated $Li[Li_{0.2}Mn_{0.54}Ni_{0.13}Co_{0.13}]O_2$ (sample (c)), and Al_2O_3-modified $Li[Li_{0.2}Mn_{0.54}Ni_{0.13}Co_{0.13}]O_2$ treated with $(NH_4)_2SO_4$ (sample (d)). XRD profiles of the samples show a characteristic pattern corresponding to Li-excess Mn-based materials, with a superlattice peak near 21° caused by the ordering of Li and Mn in the transition-metal layer. After modification and treatment, XRD peak position remained almost the

Table 1. Comparison of structure parameters of the samples

	a (Å)	c (Å)	c/a	Volume (Å^3)	R-factor
Sample (a)	2.8542	14.2175	4.9812	100.3019	0.717
Sample (b)	2.8557	14.2068	4.9748	100.3315	0.657
Sample (c)	2.8534	14.2394	4.9903	100.3997	0.482
Sample (d)	2.8551	14.2261	4.9826	100.4294	0.685

same, indicating that the modification and treatment processes did not alter the bulk structure.[9]

The surface morphology of samples (a)-(d) is shown in the SEM images in Figure 2. Primary and secondary particle sizes were measured at approximately 200-300 nm and 10-20 μm in diameter, respectively. The $(NH_4)_2SO_4$-treated $Li[Li_{0.2}Mn_{0.54}Ni_{0.13}Co_{0.13}]O_2$ substrate (sample (c)) had a rougher surface than that of the pristine substrate (sample (a)). The secondary particle size of the active material remained approximately the same before and after treatment,

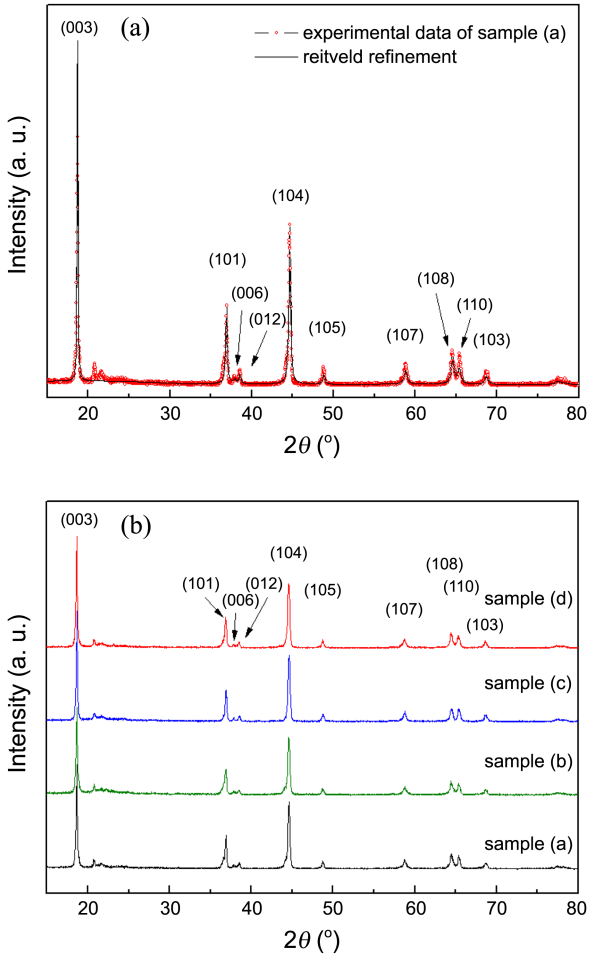

Figure 1. (a) Fitted XRD peaks of sample (a) (pristine) by rietveld refinement. (b) XRD patterns of $Li[Li_{0.2}Mn_{0.54}Ni_{0.13}Co_{0.13}]O_2$ (sample (a)), Al_2O_3-modified $Li[Li_{0.2}Mn_{0.54}Ni_{0.13}Co_{0.13}]O_2$ (sample (b)), $(NH_4)_2SO_4$-treated $Li[Li_{0.2}Mn_{0.54}Ni_{0.13}Co_{0.13}]O_2$ (sample (c)) and Al_2O_3-modified $Li[Li_{0.2}Mn_{0.54}Ni_{0.13}Co_{0.13}]O_2$ treated with $(NH_4)_2SO_4$ (sample (d)).

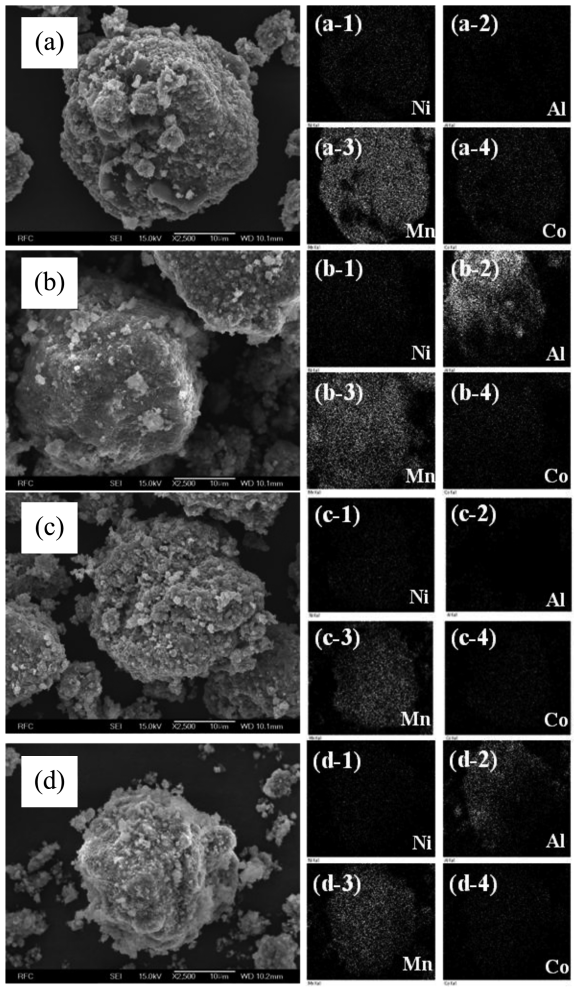

Figure 2. SEM and EDS images of (a) sample (a), (b) sample (b), (c) sample (c), and (d) sample (d).

indicating that the $(NH_4)_2SO_4$ surface treatment process did not break up the secondary particles. The Al_2O_3-modified $Li[Li_{0.2}Mn_{0.54}Ni_{0.13}Co_{0.13}]O_2$ surface (sample (b)) is smoother than the surface of the pristine substrate (sample (a)). Also, sample (d), $Li[Li_{0.2}Mn_{0.54}Ni_{0.13}Co_{0.13}]O_2$ treated with $(NH_4)_2SO_4$ and modified by coating with Al_2O_3, is smoother when compared with sample (c). EDS mapping results concerning transition metals in active materials support Al_2O_3 surface coating, as shown in Figure 2.

Figure 3(a) and (b) display TEM images confirming the Al_2O_3-coating of sample (b) and (d). The images indicated that the amorphous layer of sample (b) and (d) were coated by Al_2O_3 on the surface of cathode particles. The thickness of the coating layers in sample (b) and (d) was approximately 10 nm and 16 nm, respectively.

Figure 4(a) and (b) show the CV profiles of the samples during the first and second cycles with a scan rate of 0.03 mV/s. The samples show an initial charge peak at approximately 4.1 V and 4.6 V *vs* Li/Li$^+$, as shown in Figure 4(a). The 4.1 V peak is associated with charging of the Ni-Co-Mn component in the material, whereas the peak at 4.6 V is associated with activation of the Li_2MnO_3 component. The peaks of sample (c) and (d), active materials treated with

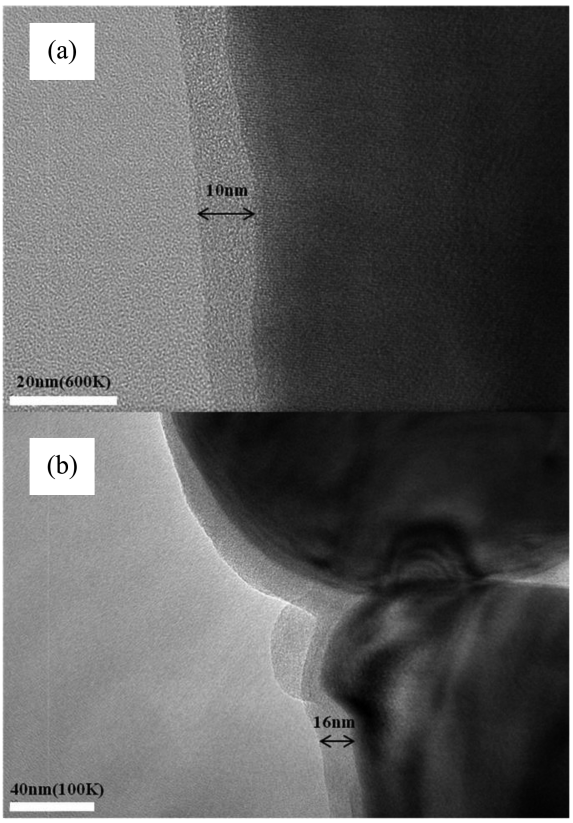

Figure 3. (a) TEM images of Al_2O_3-modified $Li[Li_{0.2}Mn_{0.54}Ni_{0.13}Co_{0.13}]O_2$ (sample (b)), (b) Al_2O_3-modified $Li[Li_{0.2}Mn_{0.54}Ni_{0.13}Co_{0.13}]O_2$ treated with $(NH_4)_2SO_4$ (sample (d)).

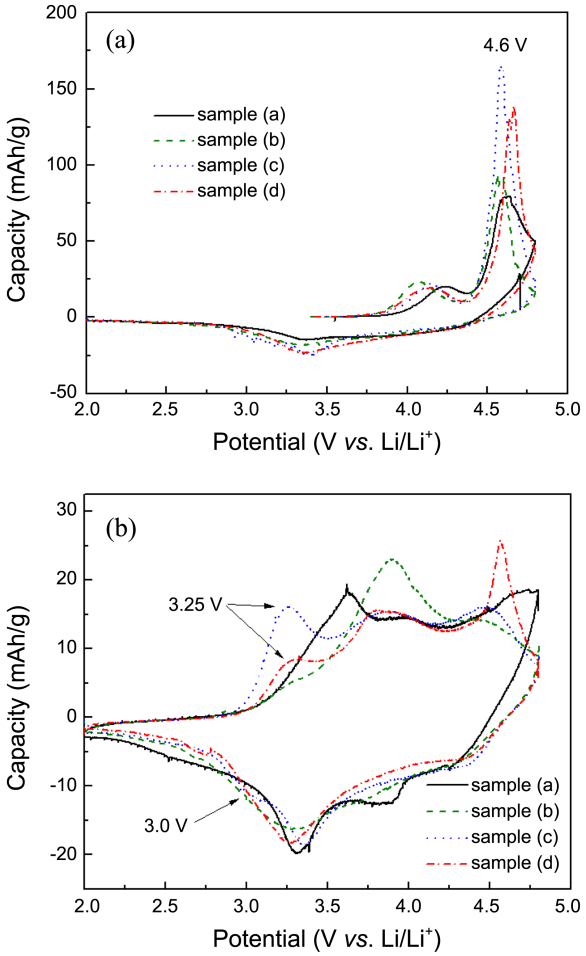

Figure 4. Cyclic voltammograms of the samples at 0.03 mV/s (a) first cycle and (b) second cycle.

$(NH_4)_2SO_4$, are higher at 4.6 V compared to sample (a) and (b) during the first cycle, suggesting a higher Li extraction rate from the Li_2MnO_3 component in the active material after $(NH_4)_2SO_4$ treatment. However, the peak for sample (d) after additional Al_2O_3-surface coating is lower than the peak of sample (c) around 4.6 V.

This is due to the existence of a boundary between the active material and the surface coating, which may limit the effectiveness of Li extraction. $(NH_4)_2SO_4$ surface treatments induce a change in structure at the surface of the active material to spinel-like regions by the exclusion of Li from

Table 2. Collected electrochemical cell data of samples

	Estimated composition	First charge capacity (mAh/g)	First discharge capacity (mAh/g)	Irreversible capacity loss (mAh/g)	Second discharge capacity (mAh/g)	100 mA/g 200 mA/g 300 mA/g capacity (mAh/g)
Sample (a)	$Li_{1.252}Mn_{0.539}Ni_{0.13}Co_{0.13}O_2$	318.4	232	86.4	229.7	210.6 197.8 188.7
Sample (b)	Al_2O_3 modified on sample (a)	317.3	232.3	85	235.1	207.8 192.8 180.4
Sample (c)	$Li_{1.132}Mn_{0.54}Ni_{0.126}Co_{0.126}O_2$	335.6	248.4	87.2	238.2	230.5 221.1 207.7
Sample (d)	Al_2O_3 modified on sample (c)	329	252.6	76.4	245.7	222.9 218.0 202.6

the active material, which is confirmed by the second cycles of CV profiles and ICP results. Figure 4(b) shows the second CV cycles for sample (c) and (d), which are the active material treated with $(NH_4)_2SO_4$. These materials have a redox pair at approximately 3.25 V and 3.0 V, marked by arrows in the figure, indicating a change in electrochemical potential. The redox pair is attributed to a spinel contribution. The improvement in rate capability is attributed to a faster Li diffusion through the spinel surface layer.[9]

Table 2 shows that Li was eliminated from the pristine material by the reaction between $Li[Li_{0.2}Mn_{0.54}Ni_{0.13}Co_{0.13}]O_2$ (pristine) and $(NH_4)_2SO_4$, as shown in the following reaction mechanism.

$$0.6Li_{4/3}Mn_{2/3}O_2 \bullet 0.4LiNi_{1/3}Co_{1/3}Mn_{1/3}O_2 + y(NH_4)_2SO_4$$

$$\rightarrow 2yNH_3 + yLi_2SO_4 + yH_2O + 0.6Li_{4/3-2y}Mn_{2/3}O_{2-y} \bullet 0.4LiNi_{1/3}Co_{1/3}Mn_{1/3}O_2$$

Surface modification by $(NH_4)_2SO_4$ decreased the ratio of Li to transition metal (Li/M), due to the formation of Li_2SO_4.

Figure 5(a) shows the first charge/discharge profiles of the cells with $Li[Li_{0.2}Mn_{0.54}Ni_{0.13}Co_{0.13}]O_2$ (sample (a)), Al_2O_3-modified $Li[Li_{0.2}Mn_{0.54}Ni_{0.13}Co_{0.13}]O_2$ (sample (b)), $(NH_4)_2SO_4$-treated $Li[Li_{0.2}Mn_{0.54}Ni_{0.13}Co_{0.13}]O_2$ (sample (c)) and Al_2O_3-modified $Li[Li_{0.2}Mn_{0.54}Ni_{0.13}Co_{0.13}]O_2$ treated with $(NH_4)_2SO_4$ (sample (d)). The voltage range is between 2.0 and 4.8 V, and the current density is 20 mA/g. Both were charged and discharged at room temperature (25 °C). Treated sample (c) and sample (d) by $(NH_4)_2SO_4$ increased the discharge-capacity compared with other samples then Al_2O_3-modified samples (d) exhibited lower irreversible capacity loss (ICL) in the first charge-discharge cycle when compared to sample (c). First cycle efficiency of sample (d) increased from about 69% for the sample (c) to over 72% with Al_2O_3 coating, due to a suppression of the reaction between the cathode surface and the electrolyte, as well as an optimization of the solid-electrolyte interface (SEI) layer.[14] The slope of the discharge curve for sample (c) shows a higher discharge potential.

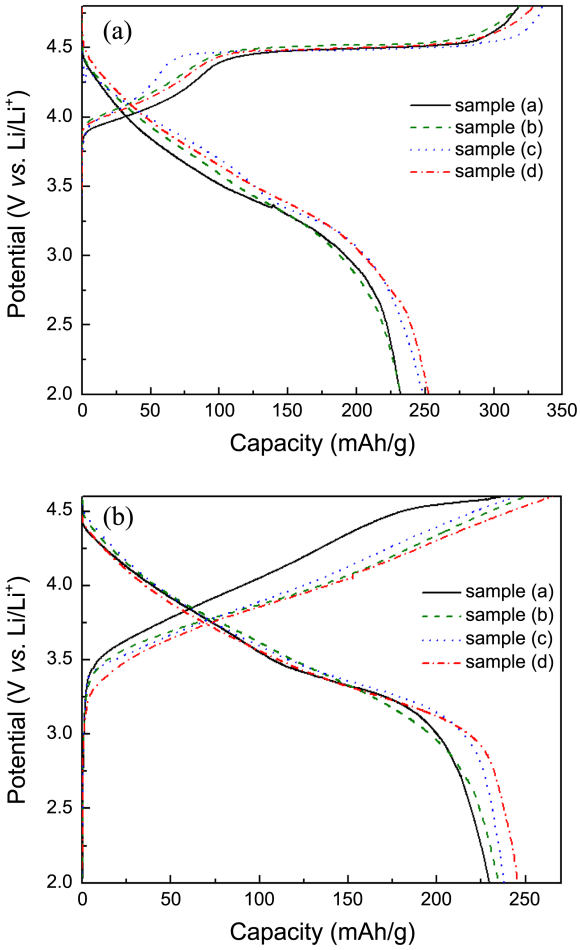

Figure 5. Charge-discharge curves of samples at 20 mA/g in the (a) first cycle and (b) second cycle.

Following the initial incline, the voltage decreased in a stair-step manner, a characteristic feature of a spinel-like component.[9] Cells were charged and discharged between 2.0 V and 4.6 V during the second cycle, as shown in Figure 5(b). Sample (d) had higher discharge capacity at ~250 mAh/g in both the first and second charge-discharge cycles. The electrochemical results are listed in Table 2.

Figure 6 shows the rate capability of the samples. Tests were performed at room temperature (25 °C) between 2.0 V and 4.6 V after the first and second cycle. The charge current was fixed at 30 mA/g, and the discharge currents were set at 100 mA/g (~0.4C), 200 mA/g (~0.8C), and 300 mA/g (~1.2C). Sample (c) and (d) showed improved rate ability after treatment with $(NH_4)_2SO_4$ when compared with the pristine substrate due to enhanced diffusion velocity, suggesting that the higher rate capability is associated with this spinel-like behavior.[9]

The rate capability of a sample (d) decreased in comparison with sample (c), because the existence of a boundary between the active material and the surface coating may limit the effectiveness of the coating. In addition, surface coating adds an inactive layer on the surface of the active material, often resulting in a decrease in the overall capacity at low rates.

A comparison of cycling performance for the prepared samples is displayed in Figure 7. The cells were cycled at a

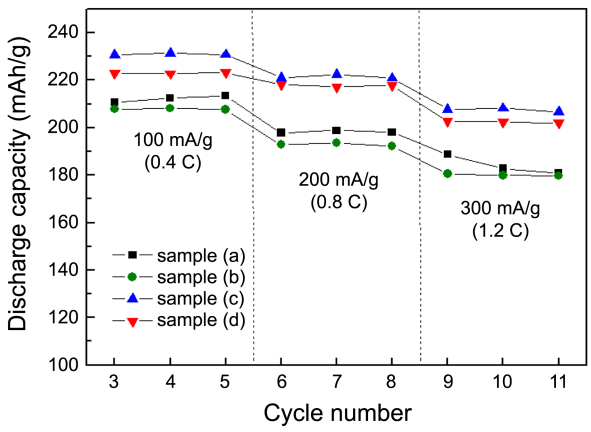

Figure 6. Rate ability of the samples at 100 mA/g, 200 mA/g, and 300 mA/g as discharge current density.

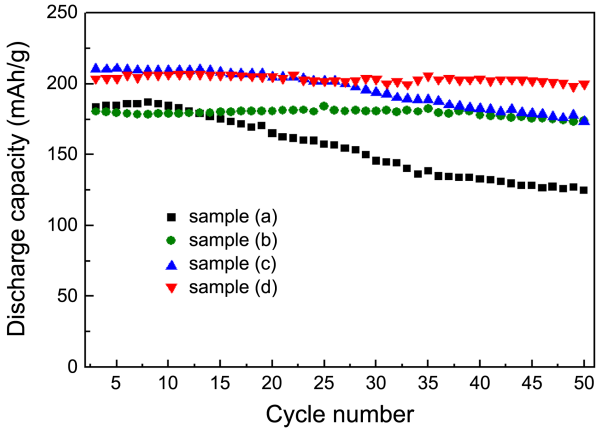

Figure 7. Cycle performance of samples at 300 mA/g as current density of discharge.

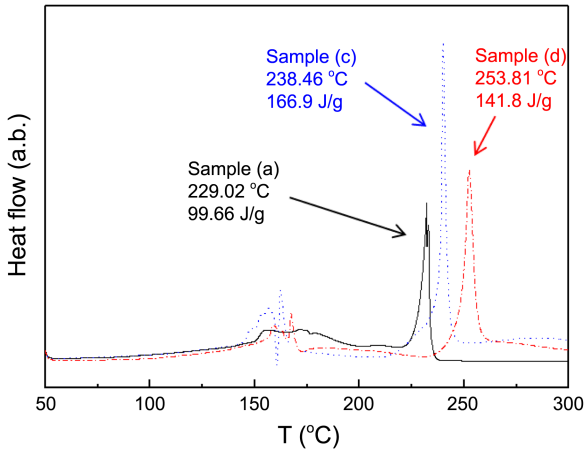

Figure 8. DSC curves of sample (a), (c), and (d).

constant current of 300 mA /g (~1.2C), with discharge in the voltage range of 2.0–4.6 V and charge current fixed at 30 mA/g. Sample (a), the pristine material, showed a dramatic decrease in discharge capacity, which was attributed to the dissolution of transition metal from the active material during cycling. The Al_2O_3-coated sample (b) and (d) showed consistent discharge capacity, as Al_2O_3 can prevent the direct contact of electrolyte solutions with cathode materials. The Al_2O_3-coated sample (d) showed an improvement in both cycle performance and enhancement of discharge capacity. For example, sample (a), (b), (c), and (d) show capacity retentions of 67.7%, 96.3%, 82.3%, and 94.7%, respectively. The results of the cycle test are listed in Table 3.

Differential scanning calorimetry was performed for comparison of thermal stability in sample (a), (c), and (d) powders, particularly in the charged 4.8 V state (Fig. 8). The exothermic peak area indicates the level of heat generation (related to oxygen generation) of the decomposed cathode following reaction with the electrolyte. Pristine, sample (a), shows a peak of decomposition at 229.02 °C (99.66 J/g). The Al_2O_3-coated sample (d) displayed an increased temperature of decomposition at 253.81 °C (141.8 J/g). The improved thermal stability of sample (d) compared to the sample (a) and (c) is due to Al_2O_3, which provides the protection of active material from reaction with electrolytes.[9,12] Sample (c) shows the onset of decomposition at 238.46 °C. This sample has the higher calorific value of approximately 166.9 J/g than the pristine and sample (d), which may be attributed to the added side reaction with electrolytes by the increased surface area from the reaction with $(NH_4)_2SO_4$. Sample (d) provides better thermal stability in the charged state.

Table 3. Cycle performances of samples at 300 mA/g after 50 cycles

	Initial discharge capacity (mAh/g)	Final discharge capacity (mAh/g)	Initial capacity over Final capacity (%)
Sample (a)	183.3	124.6	67.7
Sample (b)	180.4	173.9	96.3
Sample (c)	210.3	173.3	82.3
Sample (d)	203.6	192.9	94.7

Conclusion

The cathode material $Li[Li_{0.2}Mn_{0.54}Co_{0.13}Ni_{0.13}]O_2$ was synthesized using a co-precipitation method. In order to improve the cycle-life and thermal stability of $Li[Li_{0.2}Mn_{0.54}Co_{0.13}Ni_{0.13}]O_2$ treated with $(NH_4)_2SO_4$, substrates were surface-coated with Al_2O_3. The Al_2O_3-coated sample (d) shows lower ICL in the first charge-discharge cycle than other samples due to a suppression of the reaction between the cathode surface and the electrolyte, as well as an optimization of the SEI layer. In addition, sample (d) showed an improvement in cycle performance and an enhancement of discharge capacity (192.9 mAh/g after 50 cycles at a rate of 300 mA/g). The decrease in rate capability of sample (d), as compared to sample (c), is caused by the boundary between the active material and the surface coating, which may limit the effectiveness of the coating. In addition, surface coating adds an inactive layer on the surface of the active material. The improved thermal stability of sample (d) can be attributed to Al_2O_3, which provided protection for the active material from reaction with electrolytes. Though the Al_2O_3-coated sample (d) showed lower rate capability than sample (c), it also showed improved cycle-life and thermal stability. These results suggest that electrochemical performance depends on both surface structure and surface modification. To maintain a cycle-life and a rate capability, further work is needed to use the material with a spinel-like structure as a coating layer.

Acknowledgments. This work was supported by the 2012 Research Fund of the University of Ulsan, Ulsan, Korea.

References

1. Lu, Z.; Beaulieu, L. Y.; Donaberger, R. A.; Thomas, C. L.; Dahn, J. R. *J. Electrochem. Soc.* **2002**, *149*, A778.
2. Kang, S. H.; Sun, Y. K.; Amine, K. *Electrochem. Solid-State Lett.*

2003, *6*, A183.
3. Park, Y. J.; Hong, Y. S.; Wu, X.; Ryu, K. S.; Chang, S. H. *J. Power Sources* **2004**, *129*, 288.
4. Kang, S. H.; Amine, K. *J. Power Sources* **2003**, *124*, 533.
5. Dahn, J. R. *J. Electrochem. Soc.* **2005**, *152*, A746.
6. Jiang, J.; Eberman, K. W.; Krause, L. J.; Dahn, J. R. *J. Electrochem. Soc.* **2005**, *152*, A1879.
7. Lim, J. H.; Bang, H.; Lee, K. S.; Amine, K.; Sun, Y. K. *J. Power Sources* **2009**, *189*, 571.
8. Lee, S. H.; Koo, B. K.; Kim, J. C.; Kim, K. M. *J. Power Sources* **2008**, *184*, 276.
9. Denis, Y. W. Yu.; Katsunori, Y.; Hiroshi, N. *J. Electrochem. Soc.* **2010**, *157*, 1177.
10. Park, K. S.; Benayad, A.; Kang, D. J.; Doo, S. G. *Am. J. Chem. Soc.* **2008**, *130*, 14930.
11. Ohzuku, T.; Ueda, A.; Yamamoto, N. *J. Electrochem. Soc.* **1995**, *142*, 1431.
12. Li, C.; Zhang, H. P.; Fu, L. J.; Liu, H.; Wu, P. Y.; Rahm, E.; Holze, R.; Wu, H. Q. *Electrochim. Acta* **2006**, *51*, 3872.
13. Oh, S.; Lee, J. K.; Byuna, D.; Cho, W.; Cho, B. W. *J. Power Sources* **2004**, *132*, 249.
14. Wu, Y.; Manthiram, A. *Electrochem. Solid-State Lett.* **2006**, *9*, 221.
15. Li, C.; Zhang, H. P.; Fu, L. J.; Liu, H.; Wu, P. Y.; Rahm, E.; Holze, R.; Wu, H. Q. *Electrochim. Acta* **2006**, *51*, 3872.